ARTICLES

EPR study of Gd^{3+}-doped $RbR(SO_4)_2\cdot 4H_2O$ (R=Pr, Nd, Sm, Eu) single crystals: Phase transitions and spin-Hamiltonian parameters

Sushil K. Misra
Department of Physics, Concordia University, 1455 de Maisonneuve Boulevard West, Montreal, Quebec, Canada H3G 1M8

Lucjan E. Misiak
Department of Physics, Concordia University, 1455 de Maisonneuve Boulevard West, Montreal, Quebec, Canada H3G 1M8 and Department of Experimental Physics, Marie Curie-Sklodowska University, Place M. Curie-Sklodowska 1, 20-031 Lublin, Poland

(Received 10 December 1996; revised manuscript received 31 March 1997)

Extensive EPR measurements were carried out on Gd^{3+}-doped $RbR(SO_4)_2\cdot 4H_2O$ crystals (R=rare-earth ions, Sm, Eu, Pr, Nd) in the temperature range 100–300 K. The room-temperature data indicate that Gd^{3+} ions substitute equally for R^{3+} ions at the two magnetically inequivalent sites in the unit cell, and that the site symmetry of the Gd^{3+} ion is monoclinic. The Gd^{3+} room-temperature spin-Hamiltonian parameters and linewidths were estimated. The phase transition temperatures (T_c) were determined to be 175 ± 1 K (first order) in $RbPr(SO_4)_2\cdot 4H_2O$, 178.5 ± 1 K (first order) in $RbNd(SO_4)_2\cdot 4H_2O$, 232 ± 0.5 K (second order) in $RbSm(SO_4)_2\cdot 4H_2O$, and 230.5 ± 0.5 K (second order) in $RbEu(SO_4)_2\cdot 4H_2O$. In $RbPr(SO_4)_2\cdot 4H_2O$ and $RbNd(SO_4)_2\cdot 4H_2O$, the occurrence of the first-order phase transitions was deduced from abrupt changes in the behavior of the linewidth, zero-field splitting, and line positions, and coexistence of lines observed below and above T_c. In addition, there were observed occurrences of two more phase transitions second order in nature in $RbPr(SO_4)_2\cdot 4H_2O$ ($T_{c1}=261$ K, $T_{c2}=207.5$ K) and in $RbNd(SO_4)_2\cdot 4H_2O$ ($T_{c1}=250$ K, $T_{c2}=219.5$ K); these were not as sharply defined as the preceding ones. Below T_c, for all the crystals, the symmetry of the crystals was found to be lower than monoclinic, the four ions in the unit cell becoming magnetically inequivalent from each other. The observed second-order phase transitions in the four crystals were found to be in agreement with Landau theory of second-order phase transitions; the critical exponent was determined to be $\beta\cong 0.51$. [S0163-1829(97)03729-6]

I. INTRODUCTION

Electron paramagnetic resonance (EPR) is a sensitive tool to study the local environment about a probe ion in a crystal, e.g., structural phase transitions (SPT's), values of the spin-Hamiltonian parameters (SHP's), zero-field splitting (ZFS), and the positions and widths of EPR lines. (A review of SPT's as studied by various techniques is given in Ref. 1.) Structural phase transitions produce dynamic effects which influence the EPR spectrum of the probe ion, e.g., Gd^{3+}. Since Pr^{3+}, Nd^{3+}, Sm^{3+}, and Eu^{3+} ions have rather short spin-lattice relaxation times at higher temperatures, their EPR spectra cannot be observed in the convenient temperature region achieved with liquid nitrogen. However, the properties of the host crystals containing these ions can be monitored via the impurity ion Gd^{3+}, whose EPR spectrum can be easily recorded over a broad temperature range including room and liquid-helium temperatures. Since the Gd^{3+} ion possesses the same charge as the host Pr^{3+}, Nd^{3+}, Sm^{3+}, and Eu^{3+} ions, charge compensation is not a problem, leaving intact the mechanisms responsible for the occurrence of phase transition.

In order to understand the mechanisms responsible for SPT's, it is helpful to investigate the systematics of Gd^{3+} EPR spectra in an isostructural series of compounds. A system similar to those investigated in this paper, $NH_4R(SO_4)_2\cdot 4H_2O$ (R=rare earth), has been found to undergo at least two structural phase transitions in the range 100–300 K, as studied by specific heat measurements.[2] $NH_4R(SO_4)_2\cdot 4H_2O$ (R=Ce, Nd, Sm) crystals have also been studied by EPR,[3–6] which revealed the occurrences of structural phase transitions in $NH_4Ce(SO_4)_2\cdot 4H_2O$ (Ref. 4) and $NH_4Sm(SO_4)_2\cdot 4H_2O$ (Ref. 5) at 163 and 166 K, respectively, not detected by specific-heat measurements.[2] In the literature, there have not been reported any measurements on $RbR(SO_4)_2\cdot 4H_2O$ (RbRSTH hereafter; R=rare-earth elements Pr, Nd, Sm, Eu) crystals, other than x-ray and specific-heat (revealing a SPT occurrence at 232 K)[7] measurements on RbSmSTH single crystals. This paper reports an extensive variable-temperature EPR study of Gd^{3+}-doped RbRSTH (R=Pr, Nd, Sm, and Eu) single crystals in order to understand the lattice effects on the structural phase transitions, in addition to an estimation of spin-Hamiltonian parameters at room temperature.

II. EXPERIMENTAL ARRANGEMENT, SAMPLE PREPARATION, AND CRYSTAL STRUCTURE

EPR measurements were carried out at X band ($\sim$9.5 GHz) on a Bruker spectrometer equipped with a liquid-nitrogen variable temperature unit.[8] $RbR(SO_4)_2\cdot 4H_2O$ (R=Pr, Nd, Sm, and Eu) single crystals were grown by isothermal evaporation at room temperature from an aqueous solution of Rb_2SO_4 and $R_2(SO_4)_3\cdot 8H_2O$ mixed in the molar ratio 3:1 for R=Pr, Nd, Sm, and Eu, to which 0.5 mol % $Gd_2(SO_4)_3\cdot 8H_2O$ was added. [It was not possible to grow, $RbR(SO_4)_2\cdot 4H_2O$ single crystals for the rare-earth ions R=La, Ce, Yb, and Y.] These crystals are prismatic, with green, purple, yellow, and clear colors, indicating the presence of Pr^{3+}, Nd^{3+}, Sm^{3+}, and Eu^{3+} ions, respectively.

$RbR(SO_4)_2\cdot 4H_2O$ crystals are monoclinic, characterized by $P2_1/c$ space group symmetry.[9] The unit cell contains four formula units and its parameters are, for RbSmSTH, a =0.6565(2) nm, b=1.8913(6) nm, c=0.8728(1) nm, and β=96.26(2)°,[7] for RbEuSTH, a=0.6543(1) nm, b =1.8926(9) nm, c=0.8697(3) nm, β=96.27(5)°, for RbPrSTH, a=0.6649(2) nm, b=1.8990(7) nm, c =0.8756(2) nm, β=96.65(7)°, and for RbNdSTH, a =0.6629(1) nm, b=1.8963(5) nm, c=0.8736(1) nm, β =96.52(5)°.[9] Figure 1 displays the structure of the RbSmSTH crystal. The distances of the hydrogen-bond lengths made available by the water molecules in RbSmSTH are in the range 0.273 to 0.307 nm,[7] typical of hydrated systems in which hydrogen bonds play a crucial role in effecting cohesion of the structure to stabilize the lattice. In RbSmSTH, the Sm-O distances vary between 0.2372 and 0.2556 nm.[7] The distance between the nearest samarium ions is larger than 0.6 nm.[7] The RbRSTH structure consists of a polyhedra of R^{3+} ions, along with two crystallographically independent sulfate tetrahedra, an interlayer water molecule not coordinated to the samarium ions, and a caged Rb cation. The R^{3+} ion is coordinated to nine oxygens, six of which belong to one of the two uncoordinated sulfates and three to the waters of hydration (1), (2), and (4). The layered structure of RbRSTH is built up of chains of rare-earth coordination polyhedra, linked in directions parallel to the c axis by $S(1)O_4$ groups, and to the a-axis by $S(2)O_4$ groups. The neighbor rare-earth polyhedra parallel to the c axis are displaced along the b axis by about $\pm 1/4b$ forming continuous zigzag chains of R-polyhedra–$S(1)O_4$-tetrahedra, while the polyhedra along the a axis form continuous linear chains together with $S(2)O_4$ tetrahedra. The crystallographically independent sulfate group $S(1)O_4$ is less distorted than the $S(2)O_4$ group.[7]

III. EPR SPECTRA

Room-temperature EPR spectra indicate that of the four R^{3+} ions, there exist two magnetically inequivalent pairs of Gd^{3+} ions, referred to as GdI and GdII, hereafter, each pair consisting of two magnetically equivalent Gd^{3+} ions. The Gd^{3+} ions substitute with equal preference at the two magnetically inequivalent R^{3+}-ion sites, since the intensities of the EPR lines for the orientations of **B** along the respective Z axes of the GdI and GdII centers are equal. At each site,

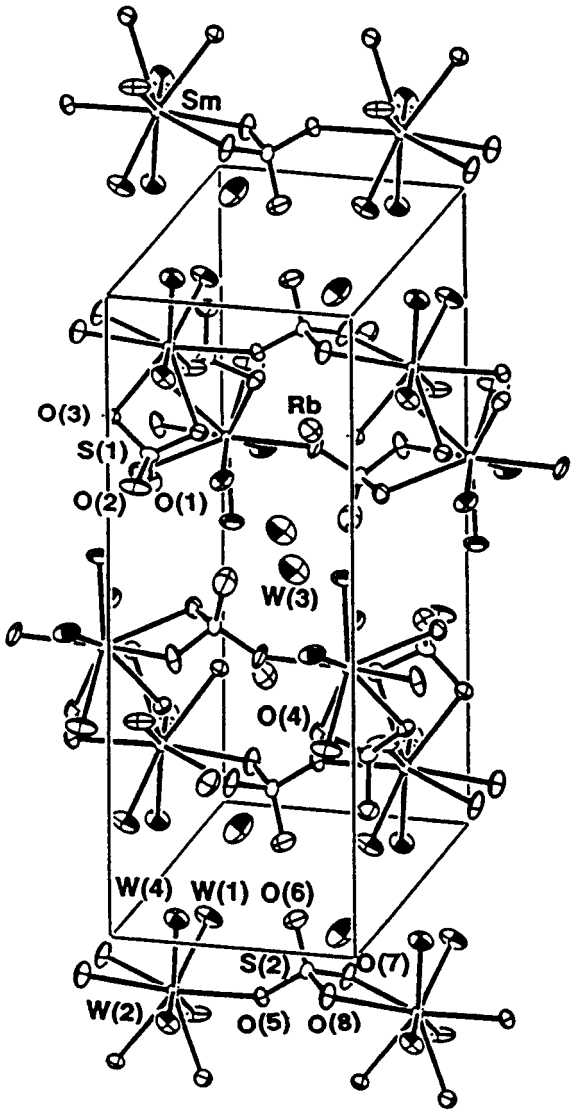

FIG. 1. Structure of $RbSm(SO_4)_2\cdot 4H_2O$. Here $W(n)$, n=1, 2, 3, 4 denote waters of hydration, $O(n)$, n=1–8, denote oxygens of sulfates, and $S(1)$ and $S(2)$ are inequivalent sulfates.[7] The structures of RbRSTH (R=Pr, Nd, Eu) are the same with Sm replaced by Pr, Nd, Eu, respectively.

the Gd^{3+} ion is characterized by monoclinic symmetry with a twofold axis of symmetry (C_{2h} or C_2) in agreement with the structure as determined by x-ray diffraction.[7,9] The intensity of the lines remains invariant with temperature.

A. Line positions

The temperature variation of EPR line positions reveal that the zero-field splitting (ZFS) varies with temperature. The monoclinic site symmetry is revealed by the angular variation of EPR lines for each site exhibiting (i) only 180° rotation symmetry and (ii) the particular behavior of angular variation of line positions in the vicinity of the principal Z and X axes, different EPR transitions attaining their extreme positions at slightly different orientations of the external magnetic field. (The magnetic Z, X, and Y axes are defined to be such that when $\mathbf{B}\|\mathbf{Z}$, $\mathbf{X}$, and $\mathbf{Y}$ axes, the positions of the various EPR transitions attain their extrema; the overall split-

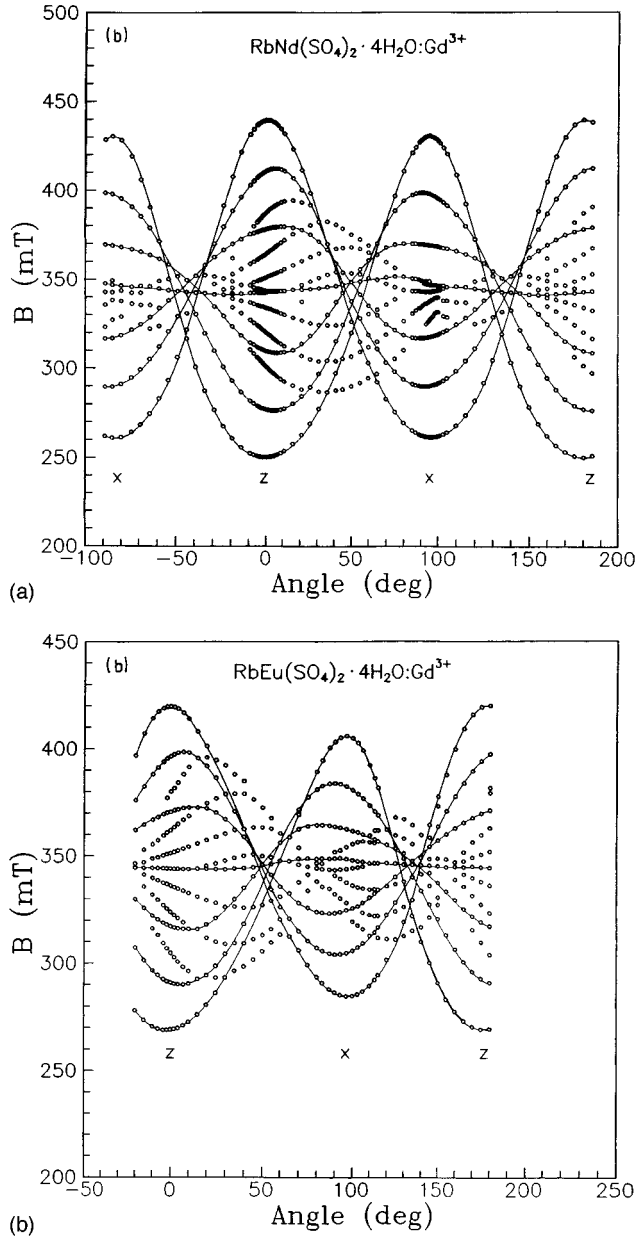

FIG. 2. Angular variation of the EPR line positions of Gd^{3+} in (a) $RbNd(SO_4)_2 \cdot 4H_2O$ and (b) $RbEu(SO_4)_2 \cdot 4H_2O$ crystals at room temperature for the orientation of the external magnetic field (**B**) in the *ZX* plane of the GdI center. Note that line positions corresponding to different transitions attain their respective extrema for different orientations of the magnetic field, and thus the rotation symmetry is 180°. This behavior is characteristic of monoclinic (C_{2h}) Gd^{3+} site symmetry. The line positions of the seven allowed lines for the GdI ion are connected by solid lines, while those for the GdII ion have been left unconnected.

ting for **B**$\|$**Z** being larger than that for **B**$\|$**X**, which in turn is larger than that for **B**$\|$**Y**.) The *Z*, *X* axes are exhibited in Figs. 2(a) and 2(b) for the Gd^{3+} ion in RbNdSTH and RbEuSTH, respectively, which exhibit an angular variation of line positions for the orientations of **B** in the magnetic *ZX* plane of the GdI center. (Those for RbPrSTH and RbSmSTH exhibit variations similar to those for RbNdSTH and RbEuSTH, respectively.) The angular differences between the maxima of the highest-field line and the line next to it for the GdI ion lie in the range of 4°–7° for all the crystals investigated here, indicating monoclinic site symmetry. For the GdII ion, this difference is much larger. It was determined that the magnetic *Z*, *X*, and *Y* axes of the GdI ion are not coincident with those of the GdII ion, similar to the situation in $NH_4R(SO_4)_2 \cdot 4H_2O$ (R=Ce, Nd, Sm) single crystals,[3–6] except that there the *Y* axes corresponding to the GdI and GdII ions are coincident. The deviation between the orientations of the *Z* and *X* axes of the GdI ion and those of the GdII ion was found to increase in the sequence R=Pr, Nd, Sm, and Eu host ions in Rb*R*STH host crystals, being about 13°, 15°, 18°, and 20°, respectively. The smaller overall splitting observed for the GdII ion for **B** parallel to its *Z* and *X* axes as compared to those for the GdI ion can be explained to be due to a small noncoincidence of the magnetic *ZX* planes of the GdI and GdII ions.

B. Linewidths

The first-derivative peak-to-peak EPR linewidths ΔB_{pp} of the Gd^{3+} ion in Rb*R*STH crystals exhibit the following behavior at 297 K. Generally, the linewidths of the GdII ion are larger than those of the GdI ion because the *ZX* plane of the GdII ion does not coincide with that for the GdI ion, the linewidths being sensitive to the orientation of **B** relative to the *Z* axis. As for the linewidths of the Gdl ion, those for the outer transitions are greater $M \leftrightarrow M-1$ ($M=\frac{7}{2}, \pm\frac{5}{2}, -\frac{3}{2}$) than those for the inner ($M=+\frac{3}{2}, \pm\frac{1}{2}$) transitions. ΔB_{pp} of the $\Delta M=\pm 1$ transitions ($M \leftrightarrow M-1$) increases as the magnitude of M increases due to the crystalline electric field, whose effect increases as one goes to the outer lines.[10] At room temperature, for the (RbPrSTH, RbNdSTH) and (RbSmSTH, RbEuSTH) hosts, the outermost lines have ΔB_{pp}'s of about 4.5 and 3.5 mT, respectively, while the central line has ΔB_{pp}'s of 2.9 and 2.5 mT, respectively. The Gd^{3+} EPR linewidths in Rb*R*STH for the members of the pairs of hosts (RbPrSTH, RbNdSTH) and (RbSmSTH, RbEuSTH) are found to be about the same. The slightly larger Gd^{3+} linewidths in RbSmSTH as compared to those in RbEuSTH is due to the magnetic moment of the Sm^{3+} ion being larger than that of the Eu^{3+} ion; thereby associated with increased contributions to linewidth by dipolar and exchange interactions between the Gd^{3+} and the host Sm^{3+} ions.

C. Temperature variation

As the temperature was lowered, the lines became very broad in the vicinity of the phase-transition temperatures. The EPR spectra as recorded for **B**$\|$**Z** of the Gd*I* ion with lowering temperature in the range 295 to $\sim$100 K are exhibited for the Rb*R*STH, R=Pr and Sm samples in Figs. 3 and 4, as typical representatives of the four crystals. The diminishing intensity of the lines marked by capital letters with temperature in these figures is due to broadening of lines. The behavior of the weaker lines, e.g., those indicated by A, B in Fig. 3 for the RbPrSTH host (and similar lines in RbNdSTH) and in Fig. 4 for RbSmSTH (and similar lines in RbEuSTH) was studied in detail; the results are presented in Figs. 5 and 6, respectively, for the RbNdSTH and RbEuSTH hosts. It was found that the widths of the lines increase with decreasing temperature above T_c for the RbSmSTH (T_c

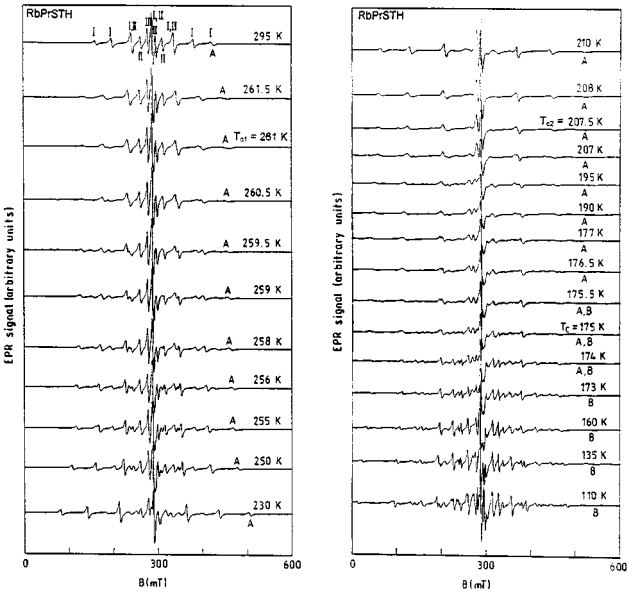

FIG. 3. EPR spectra recorded at selected temperatures above and below the phase transition temperatures ($T_{c1}=261$, $T_{c2}=207.5$, $T_c=175$ K) in a Gd^{3+}-doped $RbPr(SO_4)_2\cdot 4H_2O$ single crystal for $\mathbf{B}\|\mathbf{Z}$ of the GdI center. The spectra are selected such as to show systematically the sequence of changes as temperature is lowered.

$=232$ K) and RbEuSTH ($T_c=230.5$ K) hosts for $\mathbf{B}\|\mathbf{Z}$ of the Gd*I* ion. An examination of the Gd^{3+} spectra exhibited in the various hosts in the range 105–200 K reveal that for Rb*R*STH, the central line splits gradually into four sharp lines with lowering temperature below about 200–190 K. This is due to temperature-induced lattice deformation, making the four Gd^{3+} sites in the unit cell magnetically inequivalent, clearly displayed in Figs. 3 and 4 for RbPrSTH and

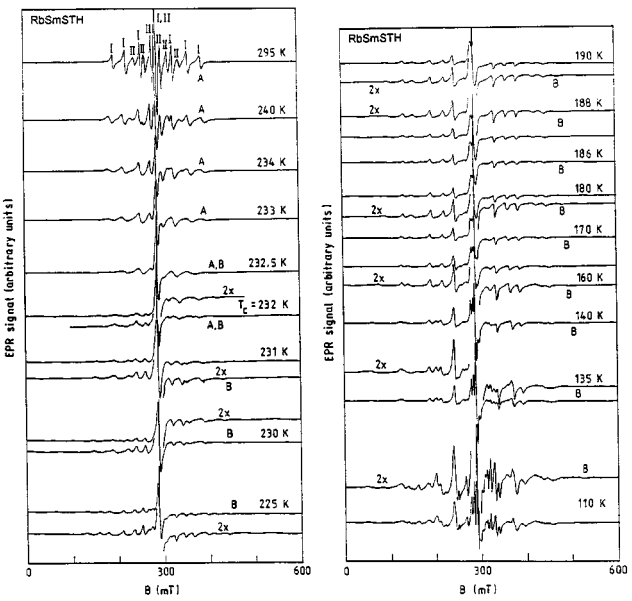

FIG. 4. EPR spectra recorded at selected temperatures above and below the phase transition temperature ($T_c=232$ K) in a Gd^{3+}-doped $RbSm(SO_4)_2\cdot 4H_2O$ single crystal for $\mathbf{B}\|\mathbf{Z}$ of the GdI center. The spectra are selected such as to show the sequence of changes as temperature is lowered.

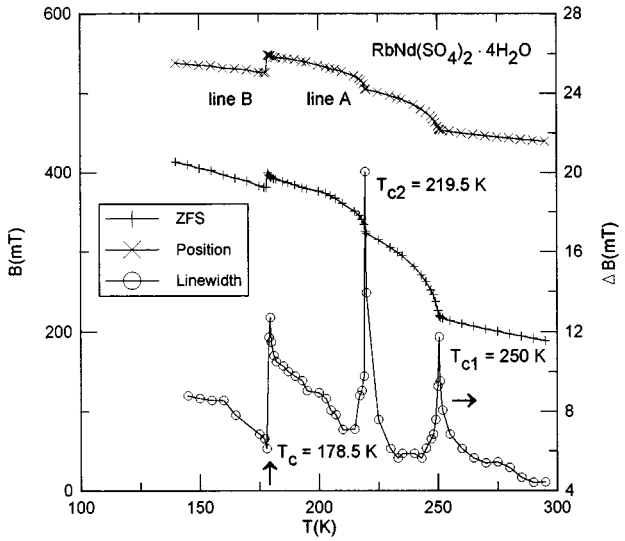

FIG. 5. Temperature variation of the zero-field splitting (ZFS), positions (B), and widths (ΔB_{pp}) of EPR lines in $RbNd(SO_4)_2\cdot 4H_2O$ crystal for $\mathbf{B}\|\mathbf{Z}$ of the GdI center. The phase transition temperature (T_c) is indicated by an arrow.

RbSmSTH at 110 and 105 K, respectively. At lower temperatures, groups of ions become polarized, destroying the pairwise physical equivalence of the four Gd^{3+} ions in the unit cell. This results in the site symmetry at the Gd^{3+} ion becoming lower from the monoclinic prevalent above T_c to triclinic below T_c. The temperature dependence of the zero-field splitting, along with the positions and widths of lines A, B, exhibited, e.g., in Figs. 5 and 6 for the RbNdSTH and RbEuSTH hosts, confirm the occurrences of structural phase transitions at temperatures marked T_c, in accordance with the temperature variation of the EPR spectra exhibited, e.g., in Figs. 3 and 4 for RbPrSTH and RbSmSTH. (See Sec. V for more details.)

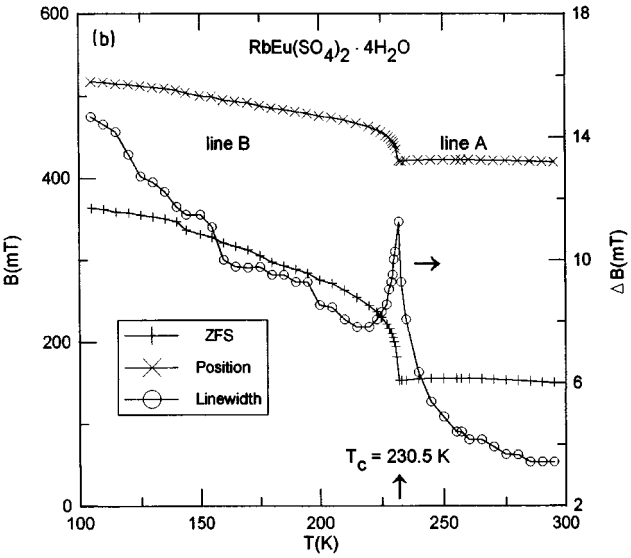

FIG. 6. Temperature variation of the zero-field splitting (ZFS), positions (B), and widths (ΔB_{pp}) of EPR lines in $RbEu(SO_4)_2\cdot 4H_2O$ crystal for $\mathbf{B}\|\mathbf{Z}$ of the GdI center. The phase transition temperature (T_c) is indicated by an arrow.

IV. SPIN HAMILTONIAN

The spin Hamiltonian used for fitting the Gd^{3+} line positions at the monoclinic site symmetry, deduced from the angular variation of line positions as discussed in Sec. III with the twofold symmetry axis parallel to the Y axis ($\mathbf{C}_2 \| \mathbf{Y}$) at room temperature in the four RbRSTH crystals is[11]

$$H = \mu_B [g_\| B_z S_z + g_\perp (B_x S_x + B_y S_y)] + \frac{1}{3} \sum_{m=0,\pm 2} b_2^m O_2^m + \frac{1}{60} \sum_{m=0,\pm 2,\pm 4} b_4^m O_4^m + \frac{1}{1260} \sum_{m=0,\pm 2,\pm 4,\pm 6} b_6^m O_6^m . \tag{4.1}$$

In Eq. (4.1), μ_B is the Bohr magneton, $S(=\frac{7}{2})$ is the electronic spin of the Gd^{3+} ion, $g_\|, g_\perp$ are the spectroscopic splitting factors, respectively, parallel and perpendicular to the symmetry axis, b_l^m are the fine-structure spin Hamiltonian parameters (SHP's) and O_l^m are the spin operators as defined by Abragam and Bleaney.[10] The monoclinic site symmetry, with the twofold axis $\mathbf{C}_2 \| \mathbf{Y}$ axis, appears to be the most plausible, as confirmed by the excellent fitting of the EPR line positions to the particular spin Hamiltonian, Eq. (4.1), given above, which consists of terms reflecting this orientation of the monoclinic axis.[11] (Monoclinic spin Hamiltonians with $\mathbf{C}_2 \| \mathbf{X}, \mathbf{Z}$ were also tried but the fits were much worse than those obtained with $\mathbf{C}_2 \| \mathbf{Y}$.) As well, it turned out that $g_{xx} = g_{yy} = g_\perp$. It is for this reason that only $g_\perp$, rather than g_{xx} and g_{yy}, were used in Eq. (4.1).

The room-temperature values of the spin-Hamiltonian-parameters (SHP's) as estimated by the use of a rigorous least-squares fitting procedure,[12] employing numerical diagonalization of the 8×8 Gd^{3+} SH matrix, fitting simultaneously all the EPR line positions for the variation of $\mathbf{B}$ in the ZX plane to the spin Hamiltonian, given by Eq. (4.1), are listed in Table I. The fitted lines are those, e.g., shown in Figs. 2(a) and 2(b) for the RbNdSTH and RbEuSTH hosts, respectively. (They are similar to those for RbPrSTH and RbSmSTH, respectively.)

TABLE I. The spin-Hamiltonian parameters (SHP's) for Gd^{3+}-doped $RbR(SO_4)_2 \cdot 4H_2O$ crystals (R = Pr, Nd, Sm, Eu) at 297 K. The g values are dimensionless, while the b_l^m's are in GHz. The errors in all parameters are ± 0.001 in appropriate units, except for b_2^0 and b_2^2, for which the error is 0.002 GHz. The root mean-square deviation per line RMSL(GHz^2) $\equiv \Sigma_i (\Delta E_i - h\nu_i)^2 / n$, where the summation is over all the n line positions fitted simultaneously to evaluate SHP's; ΔE_i and ν_i, respectively, are the separation of the energy levels participating in resonance for the ith line position and the corresponding klystron frequency; h is Planck's constant. The sign of the parameter b_2^0 has been assumed to be positive in accordance with that determined in ammonium sulfates (Refs. 4–6). It is noted that the least-squares-fitting procedure yields correct relative signs of all b_1^m.

SHP	R = Pr	R = Nd	R = Sm	R = Eu
$g_\|$	2.001	1.998	1.998	1.998
$g_\perp$	1.986	1.988	1.987	1.990
b_2^0	0.526	0.457	0.388	0.360
b_2^2	−0.392	−0.319	−0.224	−0.213
b_4^0	−0.008	−0.004	−0.002	−0.001
b_4^2	−0.019	−0.012	−0.032	−0.041
b_4^4	−0.017	−0.019	−0.020	−0.028
b_6^0	0.001	−0.001	−0.001	−0.002
b_6^2	−0.027	0.002	0.017	0.032
b_6^4	−0.053	−0.018	−0.002	0.030
b_6^6	−0.015	−0.015	−0.020	−0.005
RMSL	0.08	0.10	0.10	0.09
n	113	366	241	235

V. PHASE TRANSITIONS AND CRITICAL PHENOMENA

A. Pretransitional behavior and phase-transition temperatures (T_c)

There were observed lines that existed both above (H phase) and below (L phase) the respective phase-transition temperatures (T_c) in the four host crystals in the temperature interval ± 1.0 K. (See, e.g., Fig. 7 for the RbEuSTH host.) This behavior is similar to that detected by EPR and NMR in $RbCaF_3$ (Refs. 13–15) and by NQR in K_2OsCl_6.[16] There was found a continuous disappearance of lines belonging to the H phase and an appearance of lines belonging to the L phase as the temperature was lowered starting from 176.5, 179, 232.5, and 231 K in the RbRSTH, R = Pr, Nd, Sm, Eu crystals, respectively. The phase-transition temperature (T_c) was identified to be the middle temperature of the range over which the two phases coexist as $T_c = 175$, 178.5, 232, and 230.5 K for the RbRSTH, R = Pr, Nd, Sm, Eu crystals, respectively. In addition, as described below, in each RbRSTH (R = Pr, Nd) crystal there were observed two more phase transitions at T_{c1} and T_{c2} where the changes in the features of the EPR spectra were gradual, and not as sharp as those exhibited at T_c.

B. Behavior of linewidths in the neighborhood of T_c

The widths of the outer lines increased when approaching T_c from either higher or lower temperatures, attributed to the fluctuations in the fine-structure tensor b_2^m due to magnetic dipoles, similar to those that exist in alums.[17] ΔB_{pp}, being proportional to the inverse spin-spin relaxation time (T_2^{-1}), e.g., those of the line marked A in Figs. 3 and 4, was fitted to the expression

$$\Delta B_{pp}(T) \propto \Delta B_{pp}^0 (T - T_c)^\gamma \tag{5.1}$$

in the temperature range of about 15 K just above T_c. It yielded values of the exponent γ of -0.1, -0.1, -0.31, and -0.32 for RbRSTH, R = Pr, Nd, Sm, Eu, respectively.

As for the broadening of lines with decreasing temperature, the crystals belonging to either the pair of hosts RbPrSTH, RbNdSTH or the pair of hosts RbSmSTH,

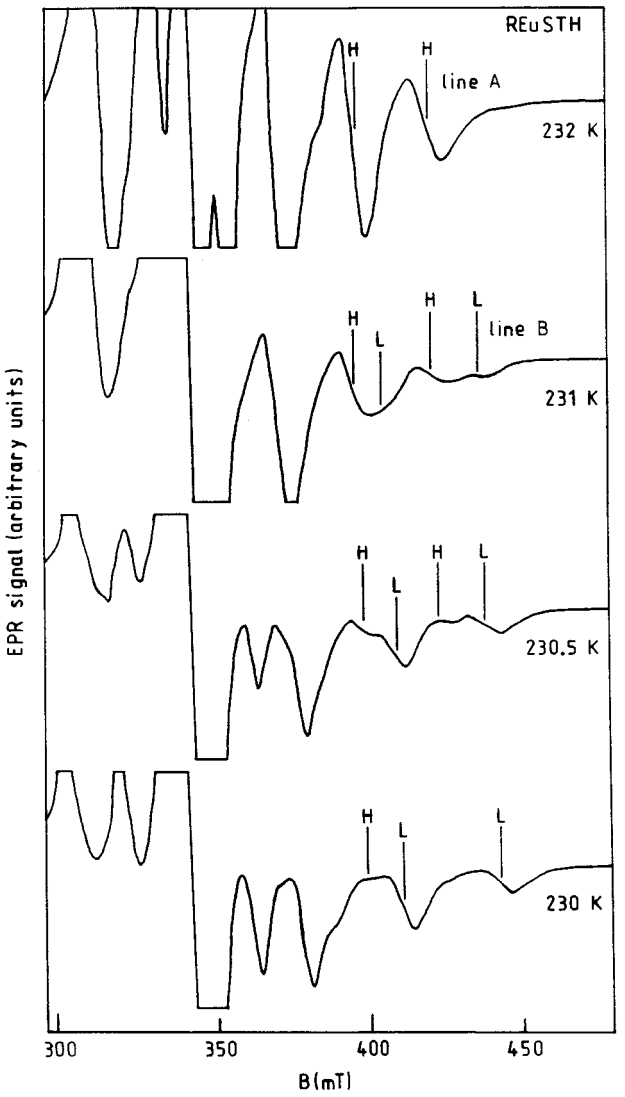

FIG. 7. EPR spectra showing simultaneous existence of lines belonging to high (H) and low (L) temperature phases for $\mathbf{B}\|\mathbf{Z}$ of the GdI center in the $RbEu(SO_4)_2\cdot 4H_2O$ crystal [similar spectra are observed for the $RbPr(SO_4)_2\cdot 4H_2O$, $RbNd(SO_4)_2\cdot 4H_2O$, and $RbSm(SO_4)_2\cdot 4H_2O$ crystals].

RbEuSTH exhibit similar behaviors, while different pairs hosts exhibit different behaviors from each other. The details are as follows.

(i) RbRSTH (R=Pr, Nd). At temperatures $T_{c1}=261$ K, $T_{c2}=207.5$ K for RbPrSTH and at $T_{c1}=250$ K, $T_{c2}=219.5$ K for RbNdSTH, there were observed drastic increases by factors of 3 (at T_{c1}) and 5 (at T_{c2}) in the linewidths as compared to those at 295 K, as determined both while warming and cooling the crystals. At T_{c1},T_{c2} there were observed splittings of the outer lines appearing suddenly in an interval of 1–1.5 K, due either to rotation of domains by a tilting of the monoclinic axis out of the ZX plane or to a deformation of the crystal lattice. In addition, lowering temperature may produce strains in the rippled layers built up of R-polyhedra–SO_4-tetrahedra chains at T_{c1} and T_{c2}, triggered by water molecules. This kind of splitting does not occur at all in the RbSmSTH and RbEuSTH crystals.

(ii) RbRSTH (R=Sm, Eu). For these crystals, broadening of the EPR lines with decreasing temperature due to dipolar interactions occurs over the entire temperature range 110–295 K. However, at respective T_c's there was observed a rapid increase of the linewidths by four times that at 295 K. This could be due to the disorder that prevails following the occurrence of a phase transition in the temperature interval of ± 15 K about T_c, similar to that observed in a Mn^{2+}-doped $Rb_2Cd_2(SO_4)_3$ crystal.[18] The directional spread of the principal axes of the b_2^0 tensors belonging to different Gd^{3+} ions due to the reorientation of tetrahedra leads to a distribution of the resonance fields of the outer fine-structure lines below T_c.

C. Shift of EPR line positions below the phase-transition temperatures

According to Landau mean-field theory of second-order phase-transitions,[19,20] the order parameter for proper transitions varies with temperature as $(T-T_c)^{\beta}$, with $\beta=0.5$. The order parameter, in the present case, is governed by the amount of angular rotation of sulfate tetrahedra[21] and Pr, Nd, Sm, or Eu polyhedra. This reflects itself as shifts in the positions of the EPR lines A and B: $\delta B\equiv(B-B_{T_{c1},T_{c2}})$ below T_{c1}, T_{c2} (line A), e.g., that shown for RbPrSTH in Fig. 3. As for RbSmSTH and RbEuSTH, this role is played by the shift of the position of line B, e.g., that shown for RbSmSTH in Fig. 4 (a similar situation is found for RbEuSTH): $\delta B=(B-B_{T_c})$. Thus,

$$\delta B\propto(T-T_{ci})^{\beta}, \tag{5.2}$$

where $T_{ci}=T_c,T_{c1},T_{c2}$ for RbPrSTH and RbNdSTH, and $T_{ci}=T_c$ for RbSmSTH and RbEuSTH.

In Eq. (5.2), the calculated values of β using experimental shifts are $\beta=0.5$ for $T_{ci}=T_{c1},T_{c2}$ and $\beta=-0.1$ (in the temperature range of 25 K just below T_c) for $T_{ci}-T_c$ for both RbRSTH (R=Pr, Nd). As for RSmSTH, REuSTH, $\beta=0.51,0.53$, respectively, in the temperature range 20 K below T_c. The excellent agreement between the experimental value of β and that predicted by Landau's theory of second-order phase transitions below T_{c1}, T_{c2} for RbRSTH (R=Pr, Nd) and below T_c for RbRSTH (R=Sm, Eu) was shown to be in conformity with the exactly solvable spherical model by Misra and Shrivastava,[22] for which $\beta=0.5$, $\gamma=2$, and $\delta=5$,[23,24] for spatial dimension $d=3$. The occurrence of the first-order phase transitions at respective T_c in RbRSTH (R=Pr, Nd) is in conformity with the fact that the EPR linewidths and shifts of lines at T_c are abrupt, characteristic of the first-order phase transition.

D. Mechanism of the second-order phase transition

Most likely, the mechanism responsible for second-order phase transitions in the four crystals presently studied is either rotation of distorted SO_4 tetrahedra, or order-disorder transition. It is difficult to distinguish between these two mechanisms. Probably the sulfate tetrahedra plays a more important role in the phase transition than do the water mol-

ecules, as they supply more (six) coordination oxygens to the R^{3+} ions than do the water molecules (three). Further, qualitatively any structural transition should exhibit order-disorder features at sufficiently small $t=(T-T_c)/T_c$.[13]

E. Trend of phase transitions occurring in the various isostructural Rb*R*STH crystals

It is interesting to note that (i) the second-order transition temperatures decrease with increasing ionic radius of the R^{3+} ions (in the order Pr, Nd, Sm, Eu) in these hosts, (ii) in Rb*R*STH (R=Sm, Eu) the EPR lines do not split before the occurrence of the phase transition, unlike Rb*R*STH (R=Pr, Nd), where they do, and (iii) in the isostructurals crystals RbErSTH and RbDySTH no phase transition has been observed to occur in the temperature range 75–295 K.[25]

VI. CONCLUDING REMARKS

The main features of the present study are as follows.

(i) Gd^{3+} ions substitute equally for R^{3+} ions at the two magnetically inequivalent sites in the unit cell at room temperature in the four crystals.

(ii) The room-temperarture zero-field splitting, and thus the spin-Hamiltonian parameters, are abnormally small in Rb *R*STH (R=Pr, Nd, Sm, Eu) as compared to those in other isostructural host crystals.

(iii) The site symmetry of the Gd^{3+} ion in Rd*R*STH (R=Pr, Nd, Sm, Edu) crystals above T_c is monoclinic, while below T_c it is lower than monoclinic, the for Gd^{3+} ions in the unit cell becoming magnetically inequivalent from each other.

(iv) The rare-earth ions do not play a significant role in the phase-transition processes, indicating that rotation or disorder of sulfate and water groups is responsible for phase transitions.

(v) First-order structural phase transition temperatures occur only in RbPrSTH and RbNdSTH at 175 ± 1 K and $T_c=178.5\pm0.5$ K, respectively, as indicated by abrupt changes in the linewidths, zero-field splitting, line positions, and coexistence of lines observed below and above T_c.

(vi) The critical exponent has been deduced to be $\beta\cong0.5$ from the shift δB of the lines in the temperature range just below T_c for Rb*R*STH (R=Sm, Eu) or just below T_{c1}, T_{c2} for Rb*R*STH (R=Pr, Nd).

(vii) The changes in the linewidth, positions of lines, and zero-field splitting occurring at the respective T_{c1} and T_{c2} temperatures in Rb*R*STH (R=Pr and Nd) crystals indicate occurrences of second-order phase transitions. The shifts of the outer line positions are in agreement with Landau theory of second-order phase transitions below T_c for Rb*R*STH (R=Sm, Eu) and below T_{c1}, T_{c2} for Rb*R*STH (R=Pr, Nd). The second-order phase transitions are either due to the rotation of SO_4 molecules triggered by water molecules or due to order-disorder transition.

It is hoped that the present EPR studies on the phase transitions occurring in Rb*R*STH (R=Pr, Nd, Sm, Eu) will stimulate further research involving specific-heat measurement, differential scanning calorimetry, Raman effect, and x-ray diffraction to develop a more in-depth understanding of the phase transitions.

ACKNOWLEDGMENTS

The authors (S.K.M., L.E.M.) are grateful to the Natural Sciences and Engineering Research Council of Canada for financial support (SKM - Grant No. OGP0004485). Support by the State Committee of Scientific Research of Poland to Marie Curie-Sklodowska University, Lublin is also acknowledged (L.E.M.).

[1] A review of the various techniques, e.g., infrared, light, and neutron scattering, NMR, NQR, and x ray, to study SPT is given by J. F. Scott, Rev. Mod. Phys. **46**, 83 (1974).
[2] S. Jasty and V. M. Malhotra, Phys. Rev. B **45**, 1 (1992).
[3] V. M. Malhotra, H. D. Bist, and G. C. Upreti, Chem. Phys. Lett. **28**, 390 (1974).
[4] V. M. Malhotra, H. A. Buckmaster, and H. D. Bist, Can. J. Phys. **58**, 1667 (1980).
[5] H. A. Buckmaster, V. M. Malhotra, and H. D. Bist, Can. J. Phys. **59**, 596 (1981).
[6] S. K. Misra, X. Li, L. E. Misiak, and C. Wang, Physica B **167**, 209 (1990).
[7] S. Jasty, P. D. Robinson, and V. M. Malhotra, Phys. Rev. B **43**, 13 215 (1991).
[8] S. K. Misra, L. E. Misiak, and J. A. Capobianco, J. Phys. Condens. Matter **6**, 3955 (1994).
[9] L. D. Iskhakova, Z. A. Starikova, E. P. Morochenets, and V. K. Trunov, Russ. J. Inorg. Chem. **24**, 854 (1979).
[10] A. Abragam and B. Bleaney, *Electron Paramagnetic Resonance of Transition Ions* (Clarendon, Oxford, 1970).
[11] S. K. Misra and C. Rudowicz, Phys. Status Solidi B **147**, 677 (1988).
[12] S. K. Misra, J. Magn. Reson. **23**, 403 (1976); S. K. Misra and S. Subramanian, J. Phys. C **15**, 7199 (1982).
[13] K. A. Müller, J. C. Fayet, F. Borsa, and A. Rigamonti, in *Structural Phase Transitions II*, edited by K. A. Müller and H. Thomas, Topics in Current Physics, Vol. 45 (Springer-Verlag, Berlin, Heidelberg, 1991).
[14] A. Trokiner, P. P. Man, H. Theveneau, and P. Papon, Solid State Commun. **55**, 929 (1985).
[15] J. Y. Buzaré, W. Berlinger, and K. A. Müller, J. Phys. (France) Lett. **46**, L201 (1985).
[16] R. L. Armstrong and M. Ramia, J. Phys. C **18**, 2977 (1975).
[17] F. J. Owens, Phys. Status Solidi B **79**, 623 (1977).
[18] S. K. Misra and S. Z. Korczak, Solid State Commun. **61**, 665 (1987).
[19] G. A. Smoleński, V. A. Bokov, V. A. Isupov, N. N. Krainik, R. E. Pasynkov, and A. I. Sokolov, in *Ferroelectrics and Related Materials*, edited by G. A. Smoleński (Gordon and Breach, New York, 1984).
[20] M. E. Lines and A. M. Glass, *Principles and Applications on Ferroelectrics and Related Materials* (Clarendon, Oxford, 1973).

[21] R. Blinc, Phys. Rep. **79**, 331 (1981).
[22] S. K. Misra and K. N. Shrivastava, Phys. Rev. B **33**, 2255 (1988).
[23] M. Wortis, in *Proceedings of the Conference on Renormalization Group*, Chestnut Hill, Pennsylvania, edited by J. D. Gunton and M. S. Green (Temple University Press, Philadelphia, 1973).
[24] G. A. Baker, Jr., H. E. Gilbert, J. Eve, and G. S. Rushbrooke, Phys. Rev. **176**, 739 (1967).
[25] S. K. Misra and L. E. Misiak (unpublished).